

# The Onset of Quark-Hadron Duality in Pion Electroproduction

T. Navasardyan,<sup>1</sup> G.S. Adams,<sup>2</sup> A. Ahmidouch,<sup>3</sup> T. Angelescu,<sup>4</sup> J. Arrington,<sup>5</sup> R. Asaturyan,<sup>1</sup> O.K. Baker,<sup>6,7</sup> N. Benmouna,<sup>9</sup> C. Bertoncini,<sup>10</sup> H.P. Blok,<sup>11</sup> W.U. Boeglin,<sup>12</sup> P.E. Bosted,<sup>13</sup> H. Breuer,<sup>8</sup> M.E. Christy,<sup>6</sup> S.H. Connell,<sup>14</sup> Y. Cui,<sup>15</sup> M.M. Dalton,<sup>14</sup> S. Danagoulian,<sup>3</sup> D. Day,<sup>16</sup> T. Dodario,<sup>15</sup> J.A. Dunne,<sup>17</sup> D. Dutta,<sup>18</sup> N. El Khayari,<sup>15</sup> R. Ent,<sup>7</sup> H.C. Fenker,<sup>7</sup> V.V. Frolov,<sup>19</sup> L. Gan,<sup>20</sup> D. Gaskell,<sup>7</sup> K. Hafidi,<sup>5</sup> W. Hinton,<sup>6,7</sup> R.J. Holt,<sup>5</sup> T. Horn,<sup>8</sup> G.M. Huber,<sup>21</sup> E. Hungerford,<sup>15</sup> X. Jiang,<sup>22</sup> M. Jones,<sup>7</sup> K. Joo,<sup>23</sup> N. Kalantarians,<sup>14</sup> J.J. Kelly,<sup>8</sup> C.E. Keppel,<sup>6,7</sup> V. Kubarovski,<sup>2</sup> Y. Li,<sup>15</sup> Y. Liang,<sup>24</sup> S. Malace,<sup>4</sup> P. Markowitz,<sup>12</sup> E. McGrath,<sup>25</sup> P. McKee,<sup>16</sup> D.G. Meekins,<sup>7</sup> H. Mkrtchyan,<sup>1</sup> B. Moziak,<sup>2</sup> G. Niculescu,<sup>16</sup> I. Niculescu,<sup>25</sup> A.K. Opper,<sup>24</sup> T. Ostapenko,<sup>26</sup> P. Reimer,<sup>5</sup> J. Reinhold,<sup>12</sup> J. Roche,<sup>7</sup> S.E. Rock,<sup>13</sup> E. Schulte,<sup>5</sup> E. Segbefia,<sup>6</sup> C. Smith,<sup>16</sup> G.R. Smith,<sup>7</sup> P. Stoler,<sup>2</sup> V. Tadevosyan,<sup>1</sup> L. Tang,<sup>6,7</sup> M. Ungaro,<sup>2</sup> A. Uzzle,<sup>6</sup> S. Vidakovic,<sup>21</sup> A. Villano,<sup>2</sup> W.F. Vulcan,<sup>7</sup> M. Wang,<sup>13</sup> G. Warren,<sup>7</sup> F. Wesselmann,<sup>16</sup> B. Wojtsekhowski,<sup>7</sup> S.A. Wood,<sup>7</sup> C. Xu,<sup>21</sup> L. Yuan,<sup>6</sup> X. Zheng,<sup>5</sup> H.Zhu<sup>16,1</sup>

<sup>1</sup> *Yerevan Physics Institute, Yerevan, Armenia*

<sup>2</sup> *Rensselaer Polytechnic Institute, Troy, New York 12180*

<sup>3</sup> *North Carolina A & T State University, Greensboro, North Carolina 27411*

<sup>4</sup> *Bucharest University, Bucharest, Romania*

<sup>5</sup> *Argonne National Laboratory, Argonne, Illinois 60439*

<sup>6</sup> *Hampton University, Hampton, Virginia 23668*

<sup>7</sup> *Thomas Jefferson National Accelerator Facility, Newport News, Virginia 23606*

<sup>8</sup> *University of Maryland, College Park, Maryland 20742*

<sup>9</sup> *The George Washington University, Washington, D.C. 20052*

<sup>10</sup> *Vassar College, Poughkeepsie, New York 12604*

<sup>11</sup> *Vrije Universiteit, 1081 HV Amsterdam, The Netherlands*

<sup>12</sup> *Florida International University, University Park, Florida 33199*

<sup>13</sup> *University of Massachusetts Amherst, Amherst, Massachusetts 01003*

<sup>14</sup> *University of the Witwatersrand, Johannesburg, South Africa*

<sup>15</sup> *University of Houston, Houston, TX 77204*

<sup>16</sup> *University of Virginia, Charlottesville, Virginia 22901*

<sup>17</sup> *Mississippi State University, Mississippi State, Mississippi 39762*

<sup>18</sup> *Triangle Universities Nuclear Laboratory and Duke University, Durham, North Carolina 27708*

<sup>19</sup> *California Institute of Technology, Pasadena, California 91125*

<sup>20</sup> *University of North Carolina Wilmington, Wilmington, North Carolina 28403*

<sup>21</sup> *University of Regina, Regina, Saskatchewan, Canada, S4S 0A2*

<sup>22</sup> *Rutgers, The State University of New Jersey, Piscataway, New Jersey, 08855*

<sup>23</sup> *University of Connecticut, Storrs, Connecticut 06269*

<sup>24</sup> *Ohio University, Athens, Ohio 45071*

<sup>25</sup> *James Madison University, Harrisonburg, Virginia 22807*

<sup>26</sup> *Gettysburg College, Gettysburg, Pennsylvania 18103*

(Dated: August 9, 2018)

A large data set of charged-pion ( $\pi^\pm$ ) electroproduction from both hydrogen and deuterium targets has been obtained spanning the low-energy residual-mass region. These data conclusively show the onset of the quark-hadron duality phenomenon, as predicted for high-energy hadron electroproduction. We construct several ratios from these data to exhibit the relation of this phenomenon to the high-energy factorization ansatz of electron-quark scattering and subsequent quark  $\rightarrow$  pion production mechanisms.

PACS numbers: 12.40.Nn, 13.87.Fh, 12.39.St, 13.60.Le

At high energies, the property of Quantum Chromodynamics (QCD) known as asymptotic freedom allows for an efficient description in terms of quarks and gluons — or partons, weakly interacting at short distances. In contrast, at low energies the effects of confinement impose a more efficient description in terms of collective degrees of freedom, the physical mesons and baryons — or hadrons.

Despite this apparent dichotomy, in nature there exist instances where low-energy hadronic phenomena, averaged over appropriate energy intervals [1], closely resemble those at asymptotically high energies, calculated in terms of quark-gluon degrees of freedom. This is referred to as quark-hadron duality, and reflects the relationship between the strong and weak interaction limits of QCD — confinement and asymptotic freedom.

The observation of this phenomenon in fact preceded QCD by a decade or so, with remarkable similarity found between the low-energy cross sections and high-energy behavior in hadronic reactions, with the former on average

appearing to mimic features of the latter. At that time, this was explained with the development of Finite Energy Sum Rules, relating dispersion integrals over resonance amplitudes at low energies to Regge parameters describing the high-energy scattering [2]. The equivalence, on average, of hadron production in electron-positron annihilation and the underlying quark-antiquark production mechanism was later similarly understood [3].

It was natural, therefore, that this same framework was used to interpret the early observation of quark-hadron duality in inclusive electron-nucleon scattering. Bloom & Gilman found that by averaging the proton  $F_2$  structure function data over an appropriate energy range, the resulting structure function in the resonance region closely resembled the scaling function which described the high-energy scattering of electrons from point-like partons [4]. Recently, the phenomenon has been revisited with unprecedented precision, and was found to work quantitatively far better, and far more locally, than could have been expected [5, 6].

Although postulated to be a general property of QCD, the dynamical origin of quark-hadron duality remains poorly understood. It should manifest itself in a wide variety of processes and observables. In this Letter, we generalize the duality concept to the unexplored region of (“semi-inclusive”) pion electroproduction [7, 8],  $eN \rightarrow e\pi^\pm X$ , in which a charged pion is detected in coincidence with a scattered electron. The missing mass of the residual system  $X$ ,  $M_x$ , is in the nucleon resonance region (defined here as  $M_x^2 < 4 \text{ GeV}^2$ ) for the remainder of this Letter, and we will show the dual behavior of this region with a high-energy parton description.

At high energies, perturbative QCD predicts factorization between the virtual photon-quark interaction and the subsequent quark hadronization,

$$\frac{\frac{d\sigma}{d\Omega_e dE_{e'} dz dp_T^2 d\phi}}{\frac{d\sigma}{d\Omega_e dE_{e'}}} = \frac{dN}{dz} b e^{-bp_T^2} \frac{1 + A\cos(\phi) + B\cos(2\phi)}{2\pi}, \quad (1)$$

$$\frac{dN}{dz} \sim \sum_q e_q^2 q(x, Q^2) D_{q \rightarrow \pi}(z, Q^2), \quad (2)$$

where the fragmentation function  $D_{q \rightarrow \pi}(z, Q^2)$  gives the probability for a quark to evolve into a pion  $\pi$  detected with a fraction  $z$  of the quark (or virtual photon) energy,  $z = E_\pi/\nu$ . The parton distribution functions  $q(x, Q^2)$  are the usual functions depending on the Bjorken variable  $x$  and  $Q^2$ . The transverse momentum  $p_T$ ,  $z$  and the angle  $\phi$  reflect the extra kinematical degree of freedom associated with the pion momentum. Both the parton distribution functions and the fragmentation functions depend on  $Q^2$  through logarithmic  $Q^2$  evolution. Their dependence on  $p_T$  is removed in a Gaussian approximation, reflected in the noted exponential  $p_T$  dependence, with  $b$  the average transverse momentum of the struck quark. In the (very) high energy limit, the factors  $A$  and  $B$  become zero. At lower energies, these “factors” reflect the longitudinal-transverse and transverse-transverse interference structure functions of the general pion electroproduction framework [9], and can, e.g., vary with  $z$  and  $Q^2$ . Note that a consequence of this factorization ansatz is that the fragmentation function is independent of  $x$ , and the parton distribution function is independent of  $z$ .

At lower energies, where hadronic phenomena dominate, it is certainly not obvious that the pion electroproduction process factorizes in the same manner as in Eq. (2). However, it has been argued that at relatively low, yet sufficiently high energies, with the quark-hadron duality phenomenon to occur, factorization may still be possible [6, 10, 11].

The experiment (E00-108) ran in the summer of 2003 in Hall C at Jefferson Lab. An electron beam with a current ranging between 20 and 60  $\mu\text{A}$  was provided by the CEBAF accelerator with a beam energy of 5.5 GeV. Incident electrons were scattered from a 4-cm-long liquid hydrogen or deuterium target and detected in the Short Orbit Spectrometer (SOS). The SOS central momentum remained constant throughout the experiment, with a value of 1.7 GeV. The electroproduced mesons (predominantly pions) were detected in the High Momentum Spectrometer (HMS), with momenta ranging from 1.3 to 4.1 GeV. The experiment consisted of two parts: i) at a fixed electron kinematics of  $(x, Q^2) = (0.32, 2.30 \text{ GeV}^2)$  the central HMS momentum was varied to cover a range of  $0.3 < z < 1.0$ ; and ii) similarly, at  $z = 0.55$ , the electron scattering angle was varied, at constant momentum transfer angle, to span a range in  $x$  from 0.22 to 0.58. Note that this corresponds to an increase in  $Q^2$ , from 1.5 to 4.2  $\text{GeV}^2$ . The invariant mass squared,  $W^2$ , is typically 5.7  $\text{GeV}^2$  and always larger than 4.2  $\text{GeV}^2$ , well in the deep inelastic region, and all measurements were performed for both  $\pi^+$  and  $\pi^-$ .

Events from the aluminum walls of the cryogenic target cell were subtracted by performing substitute empty target runs. Scattered electrons were selected by the use of both a gas Cherenkov counter and an electromagnetic calorimeter. Pions were selected using the coincidence time difference between scattered electrons and secondary hadrons. In addition, an aerogel detector was used for pion identification [12]. For kinematics with pion momenta above 2.4 GeV a correction was made to remove kaons from the pion sample, 10% in the worst case (at  $z \sim 1$ ), as determined from the electron-hadron coincidence time. From a measurement detecting positrons in SOS in coincidence with pions in

HMS, we found the background originating from  $\pi^0$  production and its subsequent decay into two photons and then electron-positron pairs, negligible.

We modelled semi-inclusive pion electroproduction [13], following the high-energy expectation of Eq. (2). We used the CTEQ5 next-to-leading-order (NLO) parton distribution functions to parameterize  $q(x, Q^2)$  [14], and the fragmentation function parameterization for  $D_{q \rightarrow \pi}^+(z, Q^2) + D_{q \rightarrow \pi}^-(z, Q^2)$ , with  $D^+$  ( $D^-$ ) the favored (unfavored) fragmentation function, from Binnewies *et al.* [15]. The remaining unknowns are the ratio of  $D^-/D^+$ , taken from a HERMES analysis [16], the slope  $b$  of the  $p_T$  dependence, and the factors  $A$  and  $B$  describing the  $\phi$  dependence.

We can not constrain  $b$  well within our own data set due to the limited  $(p_T, \phi)$  acceptance of a magnetic spectrometer setup. Here, with the possible strong correlation between the  $p_T$  and  $\phi$  dependence [17], additional assumptions are required. Hence, we will use the slope  $b$  from an empirical fit to the HERMES  $p_T$  dependence ( $b \approx 4.66 \text{ GeV}^{-2}$ ) [18]. Our own best estimate is  $b = 4.0 \pm 0.4 \text{ GeV}^{-2}$ , with no noticeable differences between  $b$ -values extracted from the  $p_T$ -dependence of either  $\pi^+$  and  $\pi^-$  data, or  $^1\text{H}$  and  $^2\text{H}$  data, somewhat lower than the HERMES slope. We do find a  $\phi$  dependence in our data, with typical parameters of  $A = 0.16 \pm 0.04$ , and  $B = 0.02 \pm 0.02$ , for an average  $\langle p_T \rangle = 0.1 \text{ GeV}$ . These  $\phi$ -dependences become smaller to negligible in the ratios of cross sections shown later. Similarly, we find a  $Q^2$ -dependence in our data that differs from the factorized high-energy expectation, but this does not affect the results shown below. Of course, these findings do cast doubt on the strict applicability of the high-energy approximation for our experiment.

Within our Monte Carlo package, we estimated two non-trivial corrections to the data. Radiative corrections were applied in two steps. We directly estimated the radiation tails within our semi-inclusive pion electroproduction data using the Monte Carlo. In addition, we explicitly subtracted radiation tails coming from the exclusive reactions  $e + p \rightarrow e' + \pi^+ + n$  and  $e + n \rightarrow e' + \pi^- + p$ . For these processes, we interpolated between the low- $W^2$ , low- $Q^2$  predictions using the MAID model [19] and the higher- $W^2$  data of Brauel *et al.* and Bebek *et al.* [20, 21]. We subtracted events from diffractive  $\rho$  production, using PYTHIA [22] to estimate the  $p(e, e' \rho^0)p$  cross section with similar modifications as implemented by the HERMES collaboration [18, 23]. We also made a 2% correction to the deuterium data to account for the loss of pions traversing the deuterium nucleus [24].

The  $^1,^2\text{H}(e, e' \pi^\pm)X$  cross sections as measured at  $x = 0.32$  are compared with the results of the simulation in Fig. 1, as a function of  $z$ . The general agreement between data and Monte Carlo is excellent for  $z < 0.65$ . Within our kinematics ( $p_T \sim 0$ ),  $M_x^2$  is almost directly related to  $z$ , as  $M_x^2 \approx M_p^2 + Q^2(1/x - 1)(1 - z)$ . Hence, the large excess at  $z > 0.8$  in the data with respect to the simulation mainly reflects the  $\gamma N - \pi \Delta(1232)$  transition region. Indeed, in *e.g.* a typical  $^1\text{H}(e, e' \pi^-)X$  spectrum one can see one prominent  $\Delta(1232)$  resonance, and only some small structure beyond [20, 21]. Apparently, above  $M_x^2 = 2.5 \text{ GeV}^2$  or so, there are already sufficient resonances to render a spectrum mimicking the smooth  $z$ -dependence as expected from the Monte Carlo simulation following the factorization ansatz of Eq. (2). Lastly, the fast drop of the simulations at large  $z$  may be artificial. Whereas fragmentation functions have been well mapped up to  $z = 0.9$  at the LEP collider [25], to better than 50%, there remain questions for semi-inclusive pion production at lower  $Q^2$ . Here, the fragmentation functions could well flatten out [26], as also included in the Field and Feynman expectations [27], that tend to produce more particles at lower energies beyond  $z = 0.7$  or so.

To quantify the surprising resemblance of semi-inclusive pion electroproduction data in the nucleon resonance region with the high energy prediction of Eq. (2), we formed simple ratios of the measured cross sections, insensitive to the fragmentation process (assuming charge symmetry) at leading order (LO) in  $\alpha_s$ . If one neglects strange quarks and any  $p_T$ -dependence to the parton distribution functions, these ratios can be expressed in terms of  $u$  and  $d$  parton distributions, as follows

$$\frac{\sigma_p(\pi^+) + \sigma_p(\pi^-)}{\sigma_d(\pi^+) + \sigma_d(\pi^-)} = \frac{4u(x) + 4\bar{u}(x) + d(x) + \bar{d}(x)}{5(u(x) + d(x) + \bar{u}(x) + \bar{d}(x))}, \quad (3)$$

$$\frac{\sigma_p(\pi^+) - \sigma_p(\pi^-)}{\sigma_d(\pi^+) - \sigma_d(\pi^-)} = \frac{4u_v(x) - d_v(x)}{3(u_v(x) + d_v(x))}, \quad (4)$$

with the notation  $\sigma_p(\pi^+)$  referring to the  $\pi^+$  pion electroproduction cross section off the proton,  $u = u_v + \bar{u}$ ,  $d = d_v + \bar{d}$ , and the  $Q^2$ -dependence left out of these formulas for convenience. These ratios allow us to study the factorization ansatz in more detail, with both ratios rendering results independent of  $z$  (and  $p_T$ ).

We show our results in Fig. 2, with the solid (open) symbols reflecting the data after (before) subtraction of the diffractive  $\rho$  contributions. The hatched areas in the bottom indicate the estimated systematic uncertainty. The shaded bands reflect the expectations under the assumptions described above (factorization, no strange quark effects, charge symmetry for the fragmentation functions), and include a variety of calculations, using both LO and NLO ( $M\bar{S}$  and valence) parton distribution functions from the GRV collaboration, and NLO calculations from the CTEQ collaboration [14, 28].

Our data are remarkably close to the near-independence of  $z$  as expected in the high-energy limit, with the clearest deviations in the region of  $z > 0.7$ , approaching on the  $\Delta(1232)$  residual mass region. Within 10% we find perfect agreement beyond this region.

Using the deuterium data only, the ratio of unfavored to favored fragmentation functions  $D^-/D^+$  can be extracted. This ratio is, to a good approximation, at LO simply given by

$$D^-/D^+ = \left(4 - \frac{\sigma_d(\pi^+)}{\sigma_d(\pi^-)}\right) / \left(4 \frac{\sigma_d(\pi^+)}{\sigma_d(\pi^-)} - 1\right). \quad (5)$$

In the high-energy limit, this ratio should solely depend on  $z$  (and  $Q^2$ ), but not on  $x$ . The results are shown in Fig. 3, with the closed (open) symbols reflecting the data after (before) subtraction of the diffractive  $\rho$  contributions. The solid curves are a fit to the HERMES data for the same ratio [16]. The dashed curve is the expectation  $(1-z)/(1+z)$  according to Field and Feynman for independent fragmentation [27]. The hatched areas indicate the systematic uncertainties, dominated by uncertainties due to the two non-trivial corrections discussed above.

We observe that the extracted values for  $D^-/D^+$  closely resemble those of the HERMES experiment [16]. The data show a near-independence as a function of  $x$ , as expected from Eq. (2), and a smooth slope as a function of  $z$ , reflecting a fit to the higher-energy HERMES data, all at  $M_x^2 > 4 \text{ GeV}^2$ . This is quite remarkable given that our data cover the full resonance region for the residual system  $X$ ,  $M_p^2 < M_x^2 < 4.2 \text{ GeV}^2$ . Apparently, there is a mechanism at work that removes the resonance excitations in the  $\pi^+/\pi^-$  ratio, and hence the  $D^-/D^+$  ratio. We note that both our data and the fit to the higher-energy HERMES data far exceed the Field and Feynman expectations for large  $z$ .

The mechanism above can be simply understood in the SU(6) symmetric quark model. Close & Isgur [11] applied this to calculate production rates in various channels in semi-inclusive pion photoproduction,  $\gamma N \rightarrow \pi X$ . The pattern of constructive and destructive interference, which was a crucial feature of the appearance of duality in inclusive structure functions, is in this model also repeated in the semi-inclusive case. The results suggest an explanation for the smooth behavior of  $D^-/D^+ \equiv D_d^{\pi^+}/D_u^{\pi^+}$  for a deuterium target in Fig. 3. The relative weights of the photoproduction matrix elements, summed over  $p$  and  $n$ , is for  $\pi^+$  production always 4 times larger than for  $\pi^-$  production. In the SU(6) limit, therefore, the resonance contributions to the ratio of Eq. (5) cancel exactly, leaving behind only the smooth background, as would be expected at high energies. This may account for the glaring lack of resonance structure in the resonance region fragmentation functions in Fig. 3.

In summary, we have measured charged-pion ( $\pi^\pm$ ) electroproduction cross sections for both hydrogen and deuterium targets. Our data cover the region where the missing mass of the residual system  $X$  is in the resonance region. We observe for the first time the quark-hadron duality phenomenon in such reactions, in that such data equate the high-energy expectations. We have quantified this behavior by constructing several ratios from these data, that exhibit, at low energies, the features of factorization in an electron-quark scattering and a subsequent quark-pion fragmentation process. Furthermore, the ratio of favored to unfavored fragmentation functions closely resembles that of high energy reactions, over the full range of missing mass. This observation can be explained in the SU(6) symmetric quark model.

The authors wish to thank A. Bruell, C.E. Carlson and W. Melnitchouk for helpful discussions. This work is supported in part by research grants from the U.S. Department of Energy, the U.S. National Science Foundation, the Natural Sciences and Engineering Research Council of Canada, and FOM (Netherlands). The Southeastern Universities Research Association operates the Thomas Jefferson National Accelerator Facility under the U.S. Department of Energy contract DEAC05-84ER40150.

- 
- [1] E.C. Poggio, H.R. Quinn and S. Weinberg, Phys. Rev. D **13** (1976) 1958.
  - [2] M. Fukugita and K. Igi, Physics Reports **31** (1977) 237.
  - [3] I.I.Y. Bigi and N. Uraltsev, Int. J. Mod. Phys. **A 16** (2001) 5201.
  - [4] E.D. Bloom and F.J. Gilman, Phys. Rev. D **4** (1971) 2901; E.D. Bloom and F.J. Gilman, Phys. Rev. Lett. **25** (1970) 1140.
  - [5] I. Niculescu *et al.*, Phys. Rev. Lett. **85** (2000) 1186; *ibid.* **85** (2000) 1182.
  - [6] W. Melnitchouk, R. Ent, and C. E. Keppel, Phys. Rep. **406** (2005) 126.
  - [7] C.K. Chen, SLAC-PUB-1469, Aug. 1974 (unpublished).
  - [8] A. Afanasev, C.E. Carlson and C. Wahlquist, Phys. Rev. D **62** (2000) 074011.
  - [9] A. S. Raskin and T. W. Donnelly, Annals Phys. **191** (1989) 78; *ibid.* **197** (1990) 202.
  - [10] N. Isgur, S. Jeschonnek, W. Melnitchouk and J.W. Van Orden, Phys. Rev. D **64** (2001) 054005.
  - [11] F.E. Close and N. Isgur, Phys. Lett. **B 509** (2001) 81.
  - [12] R. Asaturyan *et al.*, Nucl. Instrum. Meth. **A548** (2005) 364.

- [13] D. Gaskell, private communications.
- [14] H.L. Lai *et al.*, Eur. Phys. J. **C12** (2000) 375.
- [15] J. Binnewies, B. A. Kniehl, and G. Kramer, Phys. Rev. D **52** (1995) 4947.
- [16] P. Geiger, Ph.D. Dissertation, Heidelberg University (1998), unpublished.
- [17] R. N. Cahn, Phys. Lett. **B78** (1978) 269; Phys. Rev. D **40** (1989) 3107.
- [18] B. Hommez, Ph.D. Dissertation, Gent University (2003), unpublished.
- [19] D. Drechsel, S.S. Kamalov, and L. Tiator Nucl. Phys. **A645** (1999) 145.
- [20] P. Brauel *et al.*, Z. Physik C **3** (1979) 101.
- [21] C.J. Bebek *et al.*, Phys. Rev. D **17** (1978) 1693.
- [22] T. Sjostrand, L. Lonnblad, S. Mrenna, and P. Skands, hep-ph/0308153 (2003).
- [23] M. Tytgat, Ph.D. Dissertation, Gent University (2001), unpublished.
- [24] M.M. Sargsyan, private communications (2005).
- [25] S. Albino, B.A. Kniehl, and G. Kramer, Nucl. Phys. **B725** (2005) 181, and references therein.
- [26] G. Drews *et al.*, Phys. Rev. Lett. **41** (1978) 1433.
- [27] R.D. Field and R.P. Feynman, Nucl. Phys. **B136** (1978) 1.
- [28] M. Glück, E. Reya, and A. Vogt, Eur. Phys. J. **C5** (1998) 461.
- [29] M. Arneodo *et al.*, Nucl. Phys. **B321** (1989) 541.

$z$	$\sigma_p(\pi^+)$	$\sigma_p(\pi^-)$	$\sigma_d(\pi^+)$	$\sigma_d(\pi^-)$
0.321	$5.1022 \pm 0.9260$	$2.9520 \pm 0.6990$	$6.9866 \pm 1.2920$	$6.8482 \pm 3.3984$
0.335	$5.0775 \pm 0.3760$	$2.5860 \pm 0.2920$	$8.0795 \pm 0.5360$	$5.6131 \pm 1.2928$
0.349	$4.5875 \pm 0.2620$	$2.9750 \pm 0.2130$	$7.1233 \pm 0.3650$	$5.0146 \pm 0.8896$
0.363	$4.7595 \pm 0.2211$	$2.8503 \pm 0.1767$	$6.6510 \pm 0.3062$	$4.8947 \pm 0.7571$
0.377	$3.8615 \pm 0.1674$	$2.1376 \pm 0.1349$	$6.3132 \pm 0.2364$	$3.9476 \pm 0.5645$
0.391	$4.0219 \pm 0.1484$	$2.0030 \pm 0.1192$	$5.6805 \pm 0.2063$	$4.2287 \pm 0.5348$
0.405	$3.8327 \pm 0.1381$	$2.0858 \pm 0.1150$	$5.7105 \pm 0.1963$	$3.8901 \pm 0.4964$
0.419	$3.2211 \pm 0.1261$	$1.8373 \pm 0.1061$	$4.9272 \pm 0.1762$	$3.7896 \pm 0.4676$
0.433	$3.2277 \pm 0.1103$	$1.8290 \pm 0.0876$	$4.8902 \pm 0.1742$	$3.1669 \pm 0.3816$
0.447	$2.8839 \pm 0.1027$	$1.5252 \pm 0.0765$	$4.6133 \pm 0.1460$	$2.8639 \pm 0.3530$
0.461	$2.7786 \pm 0.1018$	$1.6006 \pm 0.0734$	$3.8764 \pm 0.1357$	$3.0718 \pm 0.3539$
0.475	$2.6399 \pm 0.1016$	$1.3224 \pm 0.0671$	$3.7653 \pm 0.1338$	$2.7262 \pm 0.3348$
0.489	$2.4154 \pm 0.0954$	$1.3694 \pm 0.0610$	$3.5153 \pm 0.1226$	$2.2797 \pm 0.2849$
0.503	$2.2102 \pm 0.0884$	$1.2570 \pm 0.0533$	$3.5419 \pm 0.1153$	$2.2285 \pm 0.2474$
0.517	$2.1440 \pm 0.0832$	$1.0879 \pm 0.0461$	$2.9755 \pm 0.1064$	$2.0947 \pm 0.2295$
0.531	$1.9303 \pm 0.0812$	$1.0323 \pm 0.0441$	$2.8307 \pm 0.1048$	$1.8624 \pm 0.2091$
0.545	$2.0077 \pm 0.0799$	$1.0071 \pm 0.0410$	$2.7786 \pm 0.1125$	$1.7867 \pm 0.1958$
0.559	$1.6436 \pm 0.0720$	$0.8803 \pm 0.0367$	$2.4638 \pm 0.0944$	$1.6663 \pm 0.1816$
0.573	$1.7433 \pm 0.0643$	$0.8498 \pm 0.0319$	$2.3350 \pm 0.0800$	$1.4832 \pm 0.1527$
0.587	$1.5925 \pm 0.0566$	$0.7649 \pm 0.0282$	$2.1198 \pm 0.0734$	$1.4626 \pm 0.1479$
0.601	$1.4067 \pm 0.0504$	$0.6474 \pm 0.0251$	$2.1260 \pm 0.0714$	$1.3834 \pm 0.1430$
0.615	$1.3711 \pm 0.0478$	$0.6604 \pm 0.0244$	$1.9290 \pm 0.0660$	$1.2753 \pm 0.1339$
0.629	$1.2301 \pm 0.0441$	$0.6232 \pm 0.0236$	$1.9385 \pm 0.0636$	$1.1877 \pm 0.1289$
0.643	$1.1113 \pm 0.0393$	$0.5993 \pm 0.0217$	$1.7834 \pm 0.0573$	$1.0988 \pm 0.1162$
0.657	$1.1037 \pm 0.0365$	$0.5978 \pm 0.0197$	$1.6701 \pm 0.0508$	$1.0364 \pm 0.1036$
0.671	$0.9497 \pm 0.0322$	$0.5131 \pm 0.0180$	$1.4767 \pm 0.0459$	$0.9665 \pm 0.0979$
0.685	$0.9577 \pm 0.0320$	$0.5469 \pm 0.0191$	$1.4249 \pm 0.0432$	$0.9206 \pm 0.0923$
0.699	$0.8742 \pm 0.0296$	$0.4948 \pm 0.0177$	$1.3854 \pm 0.0427$	$0.9392 \pm 0.0925$
0.713	$0.8428 \pm 0.0286$	$0.4895 \pm 0.0177$	$1.3738 \pm 0.0423$	$0.9225 \pm 0.0924$
0.727	$0.8349 \pm 0.0283$	$0.4788 \pm 0.0171$	$1.4706 \pm 0.0431$	$0.8840 \pm 0.0887$
0.741	$0.7730 \pm 0.0261$	$0.4720 \pm 0.0165$	$1.3586 \pm 0.0396$	$0.8252 \pm 0.0821$
0.755	$0.7029 \pm 0.0222$	$0.4195 \pm 0.0147$	$1.2689 \pm 0.0345$	$0.7955 \pm 0.0732$
0.769	$0.6755 \pm 0.0216$	$0.4409 \pm 0.0156$	$1.2450 \pm 0.0336$	$0.7247 \pm 0.0674$
0.783	$0.5922 \pm 0.0192$	$0.4336 \pm 0.0145$	$1.2769 \pm 0.0340$	$0.7418 \pm 0.0674$
0.797	$0.5987 \pm 0.0194$	$0.4654 \pm 0.0155$	$1.3623 \pm 0.0360$	$0.7660 \pm 0.0687$
0.811	$0.6461 \pm 0.0192$	$0.5136 \pm 0.0163$	$1.4704 \pm 0.0375$	$0.7862 \pm 0.0692$
0.825	$0.6808 \pm 0.0199$	$0.5425 \pm 0.0166$	$1.5252 \pm 0.0375$	$0.7965 \pm 0.0697$
0.839	$0.7641 \pm 0.0213$	$0.5979 \pm 0.0177$	$1.6375 \pm 0.0397$	$0.8278 \pm 0.0698$
0.853	$0.7667 \pm 0.0212$	$0.6530 \pm 0.0186$	$1.6277 \pm 0.0369$	$0.8383 \pm 0.0670$
0.867	$0.8048 \pm 0.0210$	$0.6553 \pm 0.0171$	$1.6313 \pm 0.0341$	$0.7840 \pm 0.0598$
0.881	$0.6894 \pm 0.0212$	$0.4966 \pm 0.0144$	$1.4526 \pm 0.0311$	$0.7161 \pm 0.0574$
0.895	$0.5098 \pm 0.0209$	$0.3664 \pm 0.0131$	$1.0932 \pm 0.0279$	$0.4969 \pm 0.0500$
0.909	$0.2692 \pm 0.0232$	$0.2400 \pm 0.0122$	$0.7644 \pm 0.0274$	$0.3685 \pm 0.0512$
0.923	$0.0222 \pm 0.0350$	$0.1380 \pm 0.0120$	$0.5219 \pm 0.0365$	$0.2641 \pm 0.0630$

TABLE I: Cross sections as a function of  $z$  in nb/GeV<sup>3</sup>/sr corresponding to Fig. 1. Errors are statistical only.

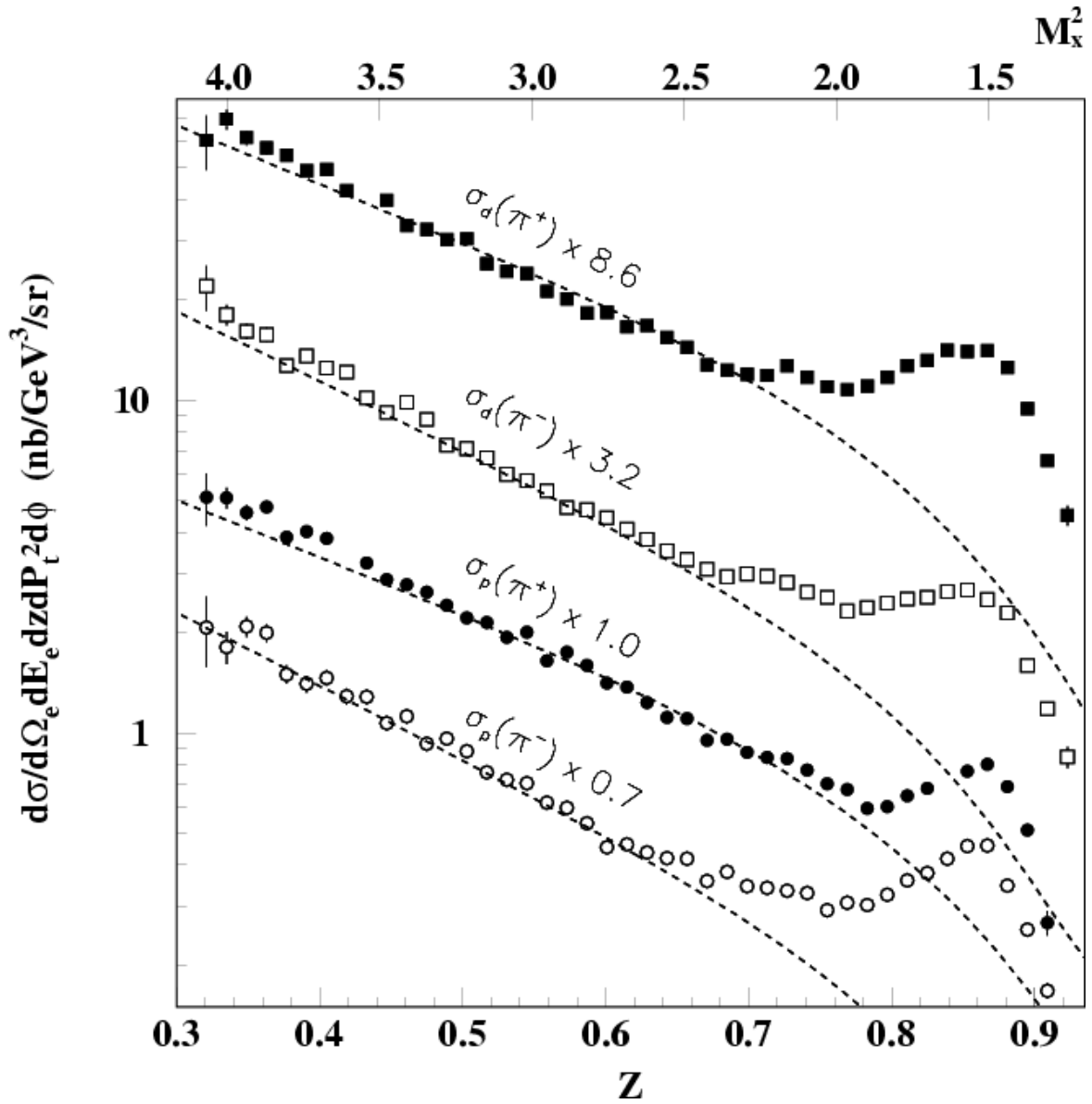


FIG. 1: The  $^{1,2}\text{H}(e, e' \pi^\pm)X$  cross sections at  $x = 0.32$  as a function of  $z$  in comparison with Monte Carlo simulations (dashed curves) starting from a fragmentation ansatz (see text). The various cross sections have been multiplied as indicated for the purpose of plotting. See Table I for numerical values.

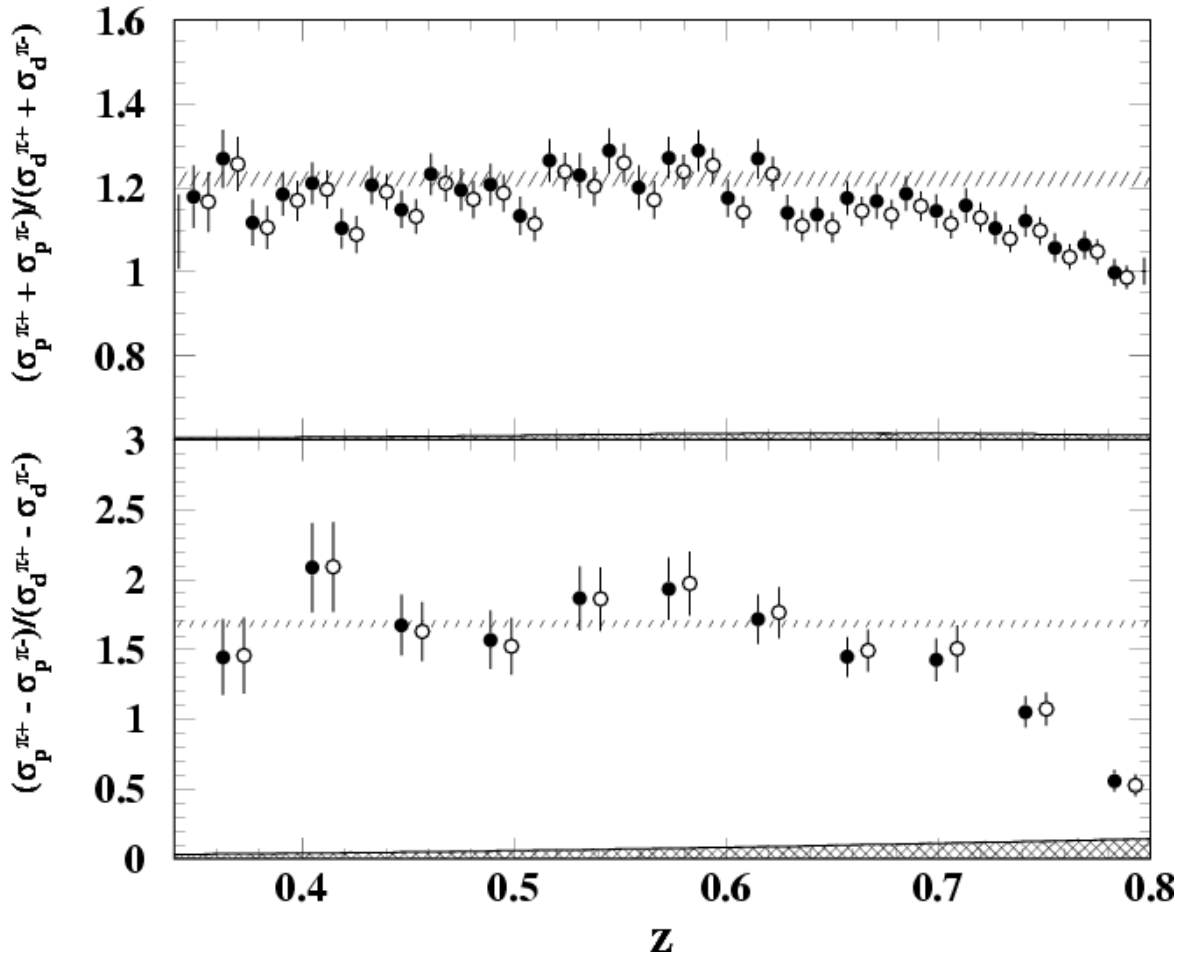


FIG. 2: The ratio of proton to deuterium results of the sum (top) and difference (bottom) of  $\pi^+$  and  $\pi^-$  cross sections as a function of  $z$ , at  $x = 0.32$ . Closed (open) symbols reflect data after (before) events from coherent  $\rho$  production are subtracted (see text). The symbols have been slightly offset in  $z$  for clarity. The hatched areas in the bottom indicate the systematic uncertainties, whereas the shaded bands represent a variety of calculations, at both leading order and next-to-leading-order of  $\alpha_s$ , of the shown ratio [14, 28]. See Tables II and III for numerical values.



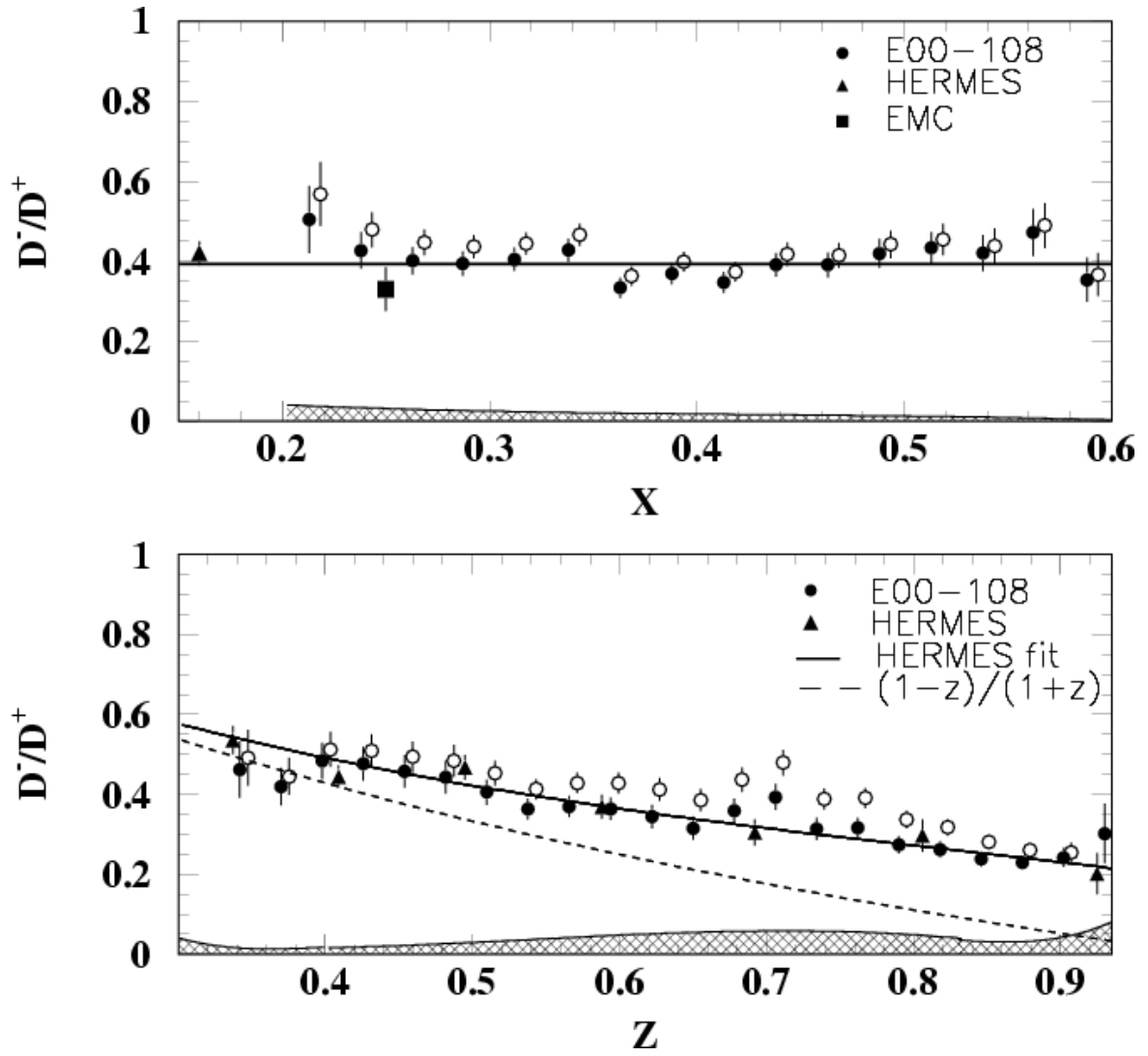


FIG. 3: *Top:* The ratio of unfavored to favored fragmentation function  $D^-/D^+$  as a function of  $x$  at  $z = 0.55$ , evaluated at leading order of  $\alpha_s$  from the deuterium data. The triangles (square) reflect HERMES (EMC) data [18, 29], with the solid curve a fit to HERMES data. Further symbols and the hatched area are as in Fig. 2. *Bottom:* Same as *top*, but now as a function of  $z$  for  $x = 0.32$ . The dashed curve represents the expectation [27] under the independent fragmentation hypothesis. See Tables IV and V for numerical values.

$z$	$R_{pd}^+$ (after $\rho$ )	$R_{pd}^+$ (before $\rho$ )
0.349	$1.1790 \pm 0.0750$	$1.1670 \pm 0.0710$
0.363	$1.2700 \pm 0.0700$	$1.2570 \pm 0.0650$
0.377	$1.1180 \pm 0.0550$	$1.1060 \pm 0.0510$
0.391	$1.1850 \pm 0.0510$	$1.1700 \pm 0.0480$
0.405	$1.2110 \pm 0.0500$	$1.1970 \pm 0.0460$
0.419	$1.1040 \pm 0.0480$	$1.0900 \pm 0.0440$
0.433	$1.2070 \pm 0.0460$	$1.1910 \pm 0.0420$
0.447	$1.1490 \pm 0.0450$	$1.1320 \pm 0.0410$
0.461	$1.2330 \pm 0.0490$	$1.2120 \pm 0.0440$
0.475	$1.1960 \pm 0.0510$	$1.1730 \pm 0.0450$
0.489	$1.2090 \pm 0.0500$	$1.1880 \pm 0.0440$
0.503	$1.1340 \pm 0.0460$	$1.1140 \pm 0.0400$
0.517	$1.2660 \pm 0.0520$	$1.2390 \pm 0.0460$
0.531	$1.2300 \pm 0.0530$	$1.2040 \pm 0.0470$
0.545	$1.2890 \pm 0.0540$	$1.2600 \pm 0.0470$
0.559	$1.2010 \pm 0.0530$	$1.1720 \pm 0.0460$
0.573	$1.2720 \pm 0.0490$	$1.2390 \pm 0.0420$
0.587	$1.2890 \pm 0.0490$	$1.2540 \pm 0.0420$
0.601	$1.1760 \pm 0.0450$	$1.1430 \pm 0.0380$
0.615	$1.2700 \pm 0.0480$	$1.2340 \pm 0.0410$
0.629	$1.1410 \pm 0.0430$	$1.1110 \pm 0.0370$
0.643	$1.1370 \pm 0.0420$	$1.1070 \pm 0.0360$
0.657	$1.1760 \pm 0.0400$	$1.1450 \pm 0.0340$
0.671	$1.1690 \pm 0.0420$	$1.1370 \pm 0.0350$
0.685	$1.1870 \pm 0.0410$	$1.1570 \pm 0.0350$
0.699	$1.1450 \pm 0.0400$	$1.1140 \pm 0.0340$
0.713	$1.1590 \pm 0.0410$	$1.1300 \pm 0.0350$
0.727	$1.1050 \pm 0.0390$	$1.0800 \pm 0.0330$
0.741	$1.1220 \pm 0.0380$	$1.0980 \pm 0.0330$
0.755	$1.0580 \pm 0.0340$	$1.0360 \pm 0.0300$
0.769	$1.0650 \pm 0.0340$	$1.0480 \pm 0.0300$
0.783	$0.9990 \pm 0.0320$	$0.9870 \pm 0.0280$

TABLE II: The ratio  $R_{pd}^+$  of proton to deuterium results of the sum of  $\pi^+$  and  $\pi^-$  cross sections as a function of  $z$ , at  $x = 0.32$ . Results reflect data after (left) or before (right) events from coherent  $\rho$  production are subtracted (see text). Errors are statistical only. The systematic error is given by  $0.0854 - 0.546z + 1.18z^2 - 0.778z^3$  for  $0.3 < z < 0.68$  and by  $-3.313 + 13.43z - 17.99z^2 + 7.995z^3$  for  $0.68 < z < 0.80$ .

$z$	$R_{pd}^-$ (after $\rho$ )	$R_{pd}^-$ (before $\rho$ )
0.363	$1.4440 \pm 0.2710$	$1.4570 \pm 0.2730$
0.405	$2.0860 \pm 0.3190$	$2.0910 \pm 0.3210$
0.447	$1.6750 \pm 0.2180$	$1.6300 \pm 0.2120$
0.489	$1.5690 \pm 0.2080$	$1.5210 \pm 0.2030$
0.531	$1.8670 \pm 0.2290$	$1.8610 \pm 0.2280$
0.573	$1.9340 \pm 0.2220$	$1.9720 \pm 0.2280$
0.615	$1.7160 \pm 0.1770$	$1.7640 \pm 0.1830$
0.657	$1.4470 \pm 0.1440$	$1.4930 \pm 0.1500$
0.699	$1.4260 \pm 0.1540$	$1.5070 \pm 0.1680$
0.741	$1.0530 \pm 0.1120$	$1.0740 \pm 0.1180$
0.783	$0.5590 \pm 0.0780$	$0.5270 \pm 0.0800$

TABLE III: The ratio  $R_{pd}^-$  of proton to deuterium results of the difference of  $\pi^+$  and  $\pi^-$  cross sections as a function of  $z$ , at  $x = 0.32$ . Results reflect data after (left) or before (right) events from coherent  $\rho$  production are subtracted (see text). Errors are statistical only. The systematic error is given by  $0.046 - 0.203z + 0.538z^2 - 0.163z^3$ .

$z$	$D^-/D^+$ (after $\rho$ )	$D^-/D^+$ (before $\rho$ )
0.342	$0.4620 \pm 0.0710$	$0.4920 \pm 0.0700$
0.370	$0.4196 \pm 0.0475$	$0.4449 \pm 0.0465$
0.398	$0.4838 \pm 0.0453$	$0.5126 \pm 0.0438$
0.426	$0.4764 \pm 0.0429$	$0.5087 \pm 0.0411$
0.454	$0.4575 \pm 0.0414$	$0.4940 \pm 0.0392$
0.482	$0.4425 \pm 0.0413$	$0.4837 \pm 0.0395$
0.510	$0.4059 \pm 0.0318$	$0.4530 \pm 0.0306$
0.538	$0.3635 \pm 0.0270$	$0.4134 \pm 0.0257$
0.566	$0.3699 \pm 0.0266$	$0.4288 \pm 0.0253$
0.594	$0.3638 \pm 0.0274$	$0.4280 \pm 0.0267$
0.622	$0.3448 \pm 0.0298$	$0.4124 \pm 0.0284$
0.650	$0.3157 \pm 0.0289$	$0.3853 \pm 0.0279$
0.678	$0.3587 \pm 0.0314$	$0.4376 \pm 0.0307$
0.706	$0.3934 \pm 0.0327$	$0.4800 \pm 0.0319$
0.734	$0.3137 \pm 0.0273$	$0.3889 \pm 0.0264$
0.762	$0.3164 \pm 0.0254$	$0.3911 \pm 0.0254$
0.790	$0.2738 \pm 0.0223$	$0.3375 \pm 0.0223$
0.818	$0.2625 \pm 0.0198$	$0.3177 \pm 0.0198$
0.846	$0.2380 \pm 0.0177$	$0.2808 \pm 0.0168$
0.874	$0.2294 \pm 0.0161$	$0.2607 \pm 0.0159$
0.902	$0.2423 \pm 0.0243$	$0.2555 \pm 0.0238$
0.930	$0.3025 \pm 0.0739$	$0.2944 \pm 0.0724$

TABLE IV: The ratio of unfavored to favored fragmentation function  $D^-/D^+$  as a function of  $z$  at  $x = 0.32$ , evaluated at leading order of  $\alpha_s$  from the deuterium data. Results reflect data after (left) or before (right) events from coherent  $\rho$  production are subtracted (see text). Errors are statistical only. The systematic error is given by  $2.445 - 18.434z + 46.196z^2 - 38.194z^3$  for  $0.2 < z < 0.3$ ,  $0.273 - 1.684z + 3.461z^2 - 2.132z^3$  for  $0.4 < z < 0.835$ , and  $-24.15 + 89.532z - 110.09z^2 + 44.974z^3$  for  $0.835 < z < 0.935$ .

$x$	$D^-/D^+$ (after $\rho$ )	$D^-/D^+$ (before $\rho$ )
0.213	$0.5048 \pm 0.0835$	$0.5682 \pm 0.0800$
0.238	$0.4272 \pm 0.0458$	$0.4789 \pm 0.0435$
0.263	$0.4008 \pm 0.0341$	$0.4472 \pm 0.0322$
0.287	$0.3939 \pm 0.0311$	$0.4361 \pm 0.0294$
0.312	$0.4049 \pm 0.0289$	$0.4446 \pm 0.0277$
0.338	$0.4278 \pm 0.0285$	$0.4660 \pm 0.0274$
0.363	$0.3334 \pm 0.0252$	$0.3631 \pm 0.0242$
0.388	$0.3690 \pm 0.0263$	$0.3987 \pm 0.0253$
0.413	$0.3476 \pm 0.0262$	$0.3732 \pm 0.0249$
0.438	$0.3914 \pm 0.0298$	$0.4177 \pm 0.0287$
0.463	$0.3907 \pm 0.0320$	$0.4142 \pm 0.0310$
0.488	$0.4198 \pm 0.0362$	$0.4420 \pm 0.0349$
0.513	$0.4336 \pm 0.0403$	$0.4546 \pm 0.0395$
0.538	$0.4202 \pm 0.0454$	$0.4385 \pm 0.0440$
0.562	$0.4721 \pm 0.0581$	$0.4890 \pm 0.0572$
0.588	$0.3533 \pm 0.0553$	$0.3668 \pm 0.0539$

TABLE V: The ratio of unfavored to favored fragmentation function  $D^-/D^+$  as a function of  $x$  at  $z = 0.55$ , evaluated at leading order of  $\alpha_s$  from the deuterium data. Results reflect data after (left) or before (right) events from coherent  $\rho$  production are subtracted (see text). Errors are statistical only. The systematic error is given by  $0.126 - 0.669x + 1.445x^2 - 1.119x^3$ .